tallic case) gap gives $2E_M = \sqrt{3}ta/(2R) = 36$ meV, where $a \approx 2.49$ Å is the lattice constant and $t \approx 2.5$ eV is the intersite hopping amplitude for graphene. In general, E_M is always comparable in scale to that of a chirality-induced gap in a nanotube of the same radius.

To compare the experimental differential conductance maps and the theoretical predictions, we note that the former are essentially a measure of density of electronic states at an energy given by the bias voltage. Figure 3 also characterizes this quantity, inasmuch as the density of lines reflects the density of states. We see from Fig. 2, A and B, that our measurements qualitatively resemble the broad predictions shown in Fig. 3A, calculated for a metallic tube. The resemblance suggests that the outer shell of sample A is intrinsically metallic. On the other hand, sample B (fig. S1) shows a similarity with simulations of semiconducting tubes (Fig. 3B), or possibly metallic and strongly doped tubes, with the Fermi level (dashed line in Fig. 3A) shifted away from the half-filled position as a result of doping. In both samples, the observed maximum gap is about an order of magnitude smaller than the estimated value $E_M = 18$ meV. Possible explanations for this include doping by impurities and intershell coupling, which can also introduce effective disorder (16, 27).

Zeeman splitting can also be observed on our SET devices, confirming the quantum dot behavior (Fig. 2B, black-and-white inset). Here we see a single energy level, which splits in the magnetic field by an amount that agrees with the g-factor reported previously for single-wall nanotubes (22). Indeed, consider, for instance, the splitting at $\Phi = 0.5\Phi_0$ (which corresponds to a field of 2.9 T), which is about 0.32 meV. This translates into a g-factor of 1.95, in agreement with previous reports (22). From these data, it is possible to estimate that the Zeeman splitting expected for $B \sim 10$ T roughly equals the maximum experimentally observed gap (0.5 to 1 meV). This explains the observation that the gap structure is not periodic with flux. This effect is clearly seen in Fig. 2A, where the periodicity with flux breaks down at high fields. Further understanding of the interplay between magnetic field–induced Zeeman and orbital effects are yet to be achieved by carrying out measurements at temperatures of a few millikelvins.

References and Notes

1. S. Iijima, *Nature* **354**, 56 (1991).
2. S. Iijima, T. Ishishashi, *Nature* **363**, 603 (1993).
3. T. W. Ebbesen *et al.*, *Nature* **382**, 54 (1996).
4. J. W. Mintmire, B. I. Dunlap, C. T. White, *Phys. Rev. Lett.* **68**, 631 (1992).
5. R. Saito, M. Fujita, G. Dresselhaus, M. S. Dresselhaus, *Appl. Phys. Lett.* **60**, 2204 (1992).
6. C. L. Kane, E. J. Mele, *Phys. Rev. Lett.* **78**, 1932 (1997).
7. R. Saito, G. Dresselhaus, M. S. Dresselhaus, *Physical Properties of Carbon Nanotubes* (Imperial College, London, 1998).
8. J. W. G. Wildoer, L. C. Venema, A. G. Rinzler, R. E Smalley, C. Dekker, *Nature* **391**, 59 (1998).
9. T. W. Odom, J.-L. Huang, P. Kim, C. M. Lieber, *Nature* **391**, 62 (1998).
10. S. Roche, G. Dresselhaus, M. S. Dresselhaus, R. Saito, *Phys. Rev. B* **62**, 16092 (2000).
11. H. Ajiki, T. Ando, *J. Phys. Soc. Jpn.* **62**, 1255 (1993).
12. J. P. Lu, *Phys. Rev. Lett.* **74**, 1123 (1995).
13. Y. Aharonov, D. Bohm, *Phys. Rev.* **115**, 485 (1959).
14. A. Bachtold *et al.*, *Nature* **397**, 673 (1999).
15. S. Frank, P. Poncharal, Z. L. Wang, W. A. de Heer, *Science* **280**, 1744 (1999).
16. S. Roche, F. Triozon, A. Rubio, D. Mayou, *Phys. Rev. B* **64**, 121401 (2001).
17. J.-O. Lee *et al.*, *Solid State Commun.* **115**, 467 (2000).
18. A. Fujiwara, K. Tomiyama, M. Yumura, K. Uchida, H. Suematsu, *Phys. Rev. B* **60**, 13492 (1999).
19. W. A. Little, R. D. Parks, *Phys. Rev. Lett.* **9**, 9 (1962).
20. Alfa Aesar, Multiwall nanotubes, Stock #43197, Lot #L03J42.
21. L. P. Kouwenhoven *et al.*, in *Mesoscopic Electron Transport*, L. L. Sohn, L. P. Kouwenhoven, G. Schön, Eds. (Kluwer, Boston, 1997), pp. 105–214.
22. S. J. Tans *et al.*, *Nature* **386**, 474 (1997).
23. H. Grabert, M. H. Devoret, Eds., *Single Charge Tunneling* (Plenum, New York, 1992).
24. M. Bockrath *et al.*, *Science* **275**, 1922 (1997).
25. The details for sample B are provided as supporting material in *Science* Online.
26. H. Ajiki, T. Ando, *J. Phys. Soc. Jpn.* **65**, 505 (1996).
27. T. Ando, *Semicond. Sci. Techol.* **15**, R13 (2000).
28. We acknowledge the technical assistance of J. Hughes and support from NSF (grant EIA01-21568), the U.S. Department of Energy (DOE) (grant DEFG02-96ER45434), and the Sloan Research Fellowship. The fabrication was done at the Frederick Seitz Materials Research Laboratory supported by DOE (grant DEFG02-91-ER45439).

Infrared Spectroscopic Evidence for Protonated Water Clusters Forming Nanoscale Cages

Mitsuhiko Miyazaki, Asuka Fujii,* Takayuki Ebata, Naohiko Mikami*

Size-dependent development of the hydrogen bond network structure in large-sized clusters of protonated water, $H^+(H_2O)_n$ (n = 4 to 27), was probed by infrared spectroscopy of OH stretches. Spectral changes with cluster size demonstrate that the chain structures at small sizes ($n \lesssim 10$) develop into two-dimensional net structures ($\sim 10 < n < 21$), and then into nanometer-scaled cages ($n \geq 21$).

Because of the fundamental importance of protonated water, $H^+(H_2O)_n$ cluster cations have been studied extensively as a microscopic model of protonated water in the condensed phase (1–11). These studies, however, have been based mainly on mass spectrometry measurements. Although the thermodynamics of $H^+(H_2O)_n$ has been extensively investigated (3, 4), structural information is still very limited, except for the small clusters, $n \leq 8$. Lee, Chang, and their co-workers carried out a detailed structural analysis of protonated water clusters using infrared (IR) spectroscopy and ab initio calculations (5–7). They determined the most stable structures for the clusters, $n \leq 6$, and they also suggested that the hydrogen bond network would develop from a chain-type structure at small cluster sizes ($n \leq 6$) to a two-dimensional (2D) net-type structure at $n \sim 7$ to 8 (7). Such hydrogen bond network structures in the protonated water clusters are substantially different from those of the neutral water clusters, $(H_2O)_n$, which form 3D cage structures even at $n = 6$ (11–13).

Very few experimental studies on structures of protonated water of $n > 8$ have been carried out. The only exception is the cluster $n = 21$, which is the well-known "magic number" in the mass distribution of $H^+(H_2O)_n$. A regular dodecahedral cage structure encaging one water molecule in the cavity has been proposed (1, 2) with support from ab initio calculations (9, 10), but no direct experimental evidence has been obtained.

We report IR spectra of size-selected protonated water clusters, $H^+(H_2O)_n$, from $n = 4$ to $n = 27$. The OH stretching vibrational region of the clusters was probed, and the formation of hydrogen-bonded 3D cage structures was demonstrated for the large-sized protonated water of $n \geq 21$.

The IR spectra of the $H^+(H_2O)_n$ cluster ions in the gas phase were measured with the tandem quadrupole mass filter–type spectrometer, described in (14), with some modifications for

Department of Chemistry, Graduate School of Science, Tohoku University, Sendai 980-8578, Japan.

*To whom correspondence should be addressed. E-mail: asuka@qclhp.chem.tohoku.ac.jp (A.F.), nmikami@qclhp.chem.tohoku.ac.jp (N.M.)

the present work (*15*). Cluster cations of a specific size, which were size-selected by the first of two quadrupole mass filters, were introduced into an octopole ion guide. The cluster cations were irradiated by counter-propagating IR light in the ion guide. When the IR light was resonant with a vibrational transition of the cluster cation, vibrational predissociation resulted in fragmentation of the cluster cation. A second quadrupole mass filter was tuned to pass only the $(n-1)$ or $(n-2)$ fragment cluster cations. IR spectra were recorded by scanning the IR wavelength while monitoring the intensity of the fragment cations. IR light was generated by difference-frequency generation (DFG) between the fundamental outputs of a Nd:YAG (Nd:yttrium-aluminum-garnet) laser and a dye laser.

The IR spectra of $H^+(H_2O)_n$ ($n = 4$ to 27) in the 3-μm region (Fig. 1) show broad features below 3600 cm^{-1} that we attribute to hydrogen-bonded OH stretching vibrations. We assigned the relatively sharp bands above 3600 cm^{-1} to free OH stretching vibrations (expanded scale, Fig. 2). The spectral gap in the region of 3460 to 3520 cm^{-1} is caused by the depletion of the IR laser power by water impurities in the DFG crystal. Additionally, sharp dips in the spectra above 3520 cm^{-1} (more noticeable in Fig. 2) resulted from IR absorptions due to atmospheric water in the optical path. In the spectra of the clusters larger than $n = 21$, fluctuation of the parent-cluster ion intensity caused sharp dips throughout the whole spectral region. IR spectra of $H^+(H_2O)_n$ ($n = 4$ to 8) clusters have been reported by Lee, Chang, and co-workers (*5–7*), and the present spectra show essentially the same features except for somewhat broader bandwidths arising from hot bands and structural isomers. Lee *et al.* have estimated their cluster beam temperature to be about 170 K (*7*). The broader bandwidths observed in the present spectra suggest a much higher internal temperature (energy) of the clusters, and many structural isomers may contribute to the present spectra (*16*). With an increase in the cluster size, however, the IR spectra show gradual changes in both the free and hydrogen-bonded OH stretch regions. Such spectral changes reflect a general trend toward a hydrogen bond network structure that strongly depends on cluster size.

Detailed cluster structures up to $n = 6$ were determined by Jiang *et al.* (*7*). For these cluster sizes, the H_3O^+ or $H_5O_2^+$ ion core is located at the center of the cluster, and radial hydrogen bond chains originate from this three- or four-coordinated ion core, as schematically shown in Fig. 3A. The water molecule that terminates the hydrogen bond chain is a single proton acceptor (A-water), and its symmetric (ν_1) and antisymmetric (ν_3) stretching vibrations of free OH bonds appear at ~3640 and ~3740 cm^{-1}, respectively. A

hydrogen bond chain is composed of two-coordinated water molecules of single acceptor–single donor (AD-water molecules). The hydrogen-bonded OH stretches in such an AD-water site occur at ~3400 cm^{-1}, whereas the dangling OH stretch appears at 3715 cm^{-1} (*7, 17, 18*).

Above $n = 6$, an obvious spectral change occurs in the free-OH stretch region (Fig. 2). The ν_1 and ν_3 bands of the terminal A-water show a gradual high-frequency shift with increasing cluster size, reflecting the increase in distance from the charge center. Moreover, the intensity of these bands decreases with cluster size, and the bands finally disappear at $n \sim 10$. At the same time as this decrease, a new band starts to appear at ~3690 cm^{-1} that has been assigned to the dangling OH

stretching vibration in a three-coordinated water molecule of double acceptor–single donor (AAD-water molecule) (*17–21*). This assignment has been made on the basis of IR spectroscopy and ab initio calculations of smaller-sized protonated water clusters, and it has also been proposed in ice surface studies. Such a three-coordinated water molecule occurs at a bridging site of hydrogen bond chains. The disappearance of A-water bands and simultaneous appearance of AAD-water bands for clusters $n = 7$ to 10 indicates the development of the hydrogen network from the chain type to a 2D net structure (Fig. 3, A and B). With a donation of one proton, a terminal A-water molecule is bound to an AD-water molecule in a hydrogen bond chain. Then, the terminal A-water molecule is
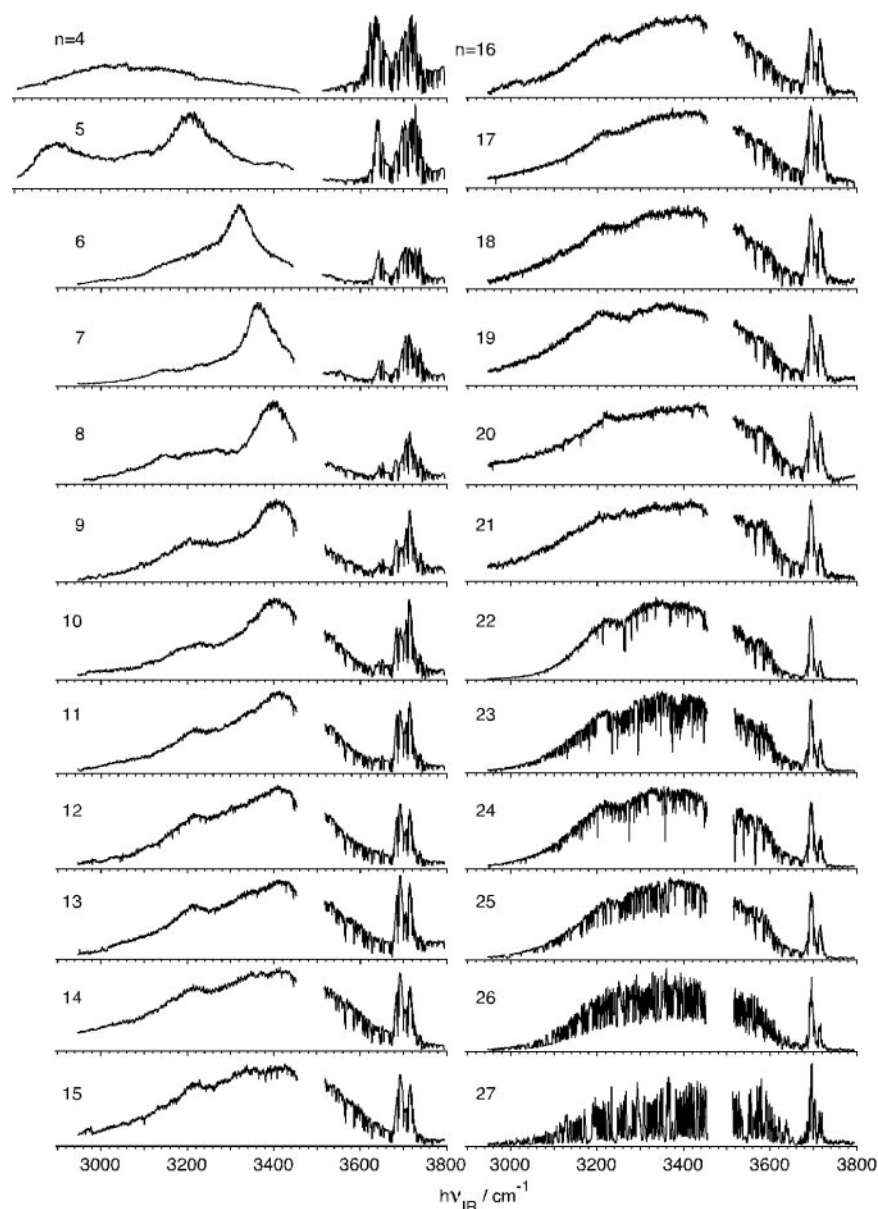

Fig. 1. IR spectra of size-selected protonated water-cluster cations, $H^+(H_2O)_n$ ($n = 4$ to 27), in the OH stretching vibrational region.

transformed to an AD-water molecule in a chain, and the AD-water molecule results in an AAD-water molecule at the bridging site of the chains. When all of the terminal water molecules are bound, the A-water bands disappear, and the hydrogen bond network is rearranged into a 2D net structure that consists only of AD- and AAD-water molecules. In accordance with this change, a new band appears in the spectral region 3200 cm^{-1} for the clusters $n \geq 7$. This band can be assigned to the hydrogen-bonded OH stretch of the AAD-water molecule, which is expected to appear at ~3050 cm^{-1} (20–22). However, alternative assignments, such as the overtone

of an OH bending vibration or a hydrogen-bonded OH stretch of the $H_5O_2^+$ ion core (7), are also possible for this band.

In the clusters from $n = 10$ to $n = 19$, the IR spectra of the free-OH stretch region show two bands of almost equal intensity at 3695 and 3715 cm^{-1} due to the dangling OH stretches of AAD- and AD-water molecules, respectively. The hydrogen-bonded OH region shows only a small modulation in the band feature. These spectral features show that the hydrogen bond network preserves a 2D net structure for these cluster sizes.

From $n \gtrsim 19$, new spectral features representing the next stage of network growth were

observed. A shoulder at ~3580 cm^{-1} starts to appear as a new absorption band, which is assigned to hydrogen-bonded OH stretching vibrations of three-coordinated water molecules of single acceptor–double donor (ADD-water molecule) (20, 21). At the same time as the new band appears, the intensity of the dangling OH stretch band of AD-water at 3715 cm^{-1} gradually decreases with increasing cluster size. Although the intensity of the AD-water OH stretch remains as strong as that of the AAD-water for $n \leq 19$, it is substantially weaker than that of the AAD-water OH stretch for $n \geq 21$. Such spectral changes indicate a decrease in the number of AD-water sites and a corresponding increase in the number of ADD- and AAD-water sites. That is, an AD-water molecule is transformed to an ADD-water molecule by donation of the remaining dangling OH bond to
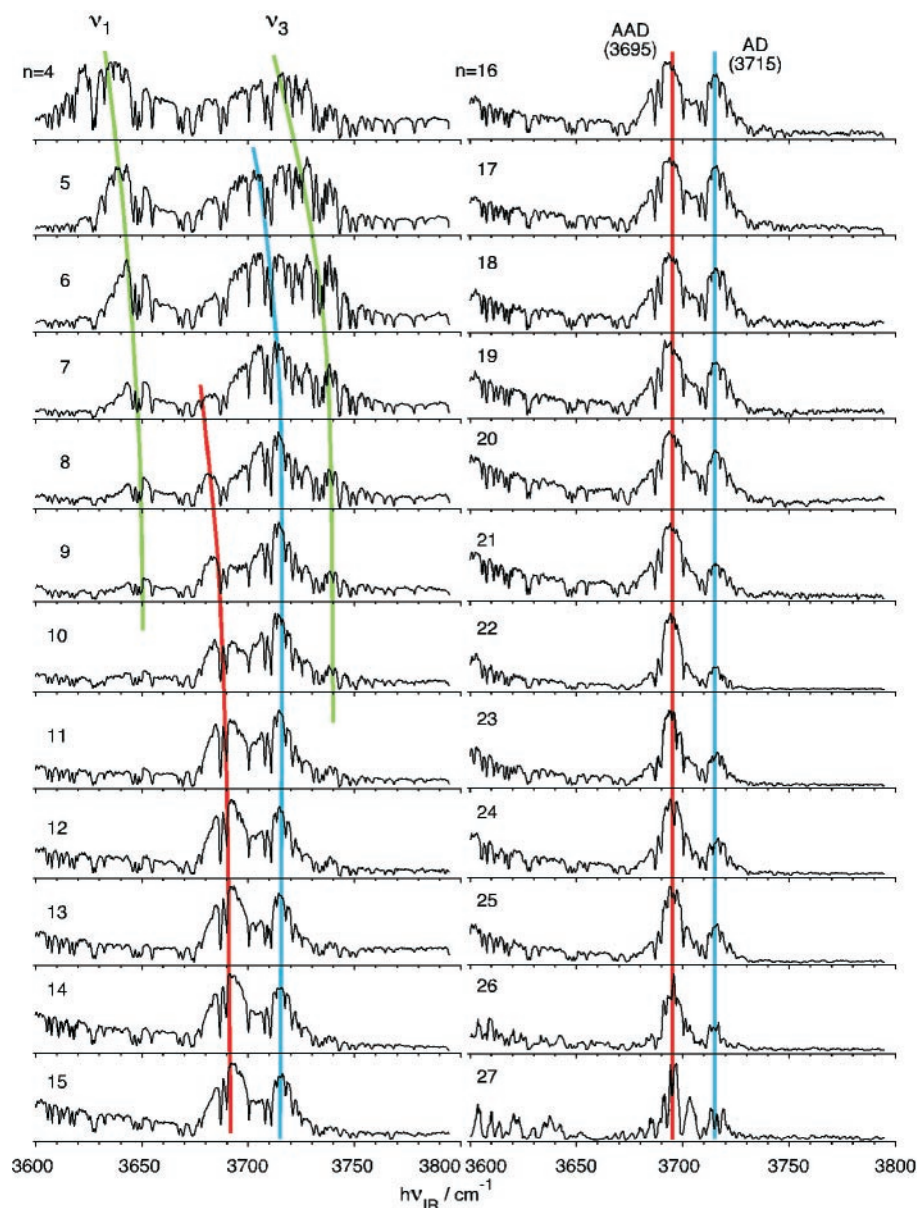

Fig. 2. Free OH stretching vibrational region of the IR spectra of H$^+$(H$_2$O)$_n$ ($n = 4$ to 27). Four different types of free OH stretching vibrations are seen. Bands at 3640 and 3740 cm^{-1} (indicated by green lines) are ν_1 and ν_3 vibrations of a terminal (A-) water molecule of a hydrogen bond chain. Bands at 3695 cm^{-1} (red line) and 3715 cm^{-1} (blue line) are attributed to dangling OH stretches of three-coordinated (AAD-) and two-coordinated (AD-) water molecules, respectively (see text). Sharp dips in the spectra are due to the absorption of the atmospheric water in the optical path.
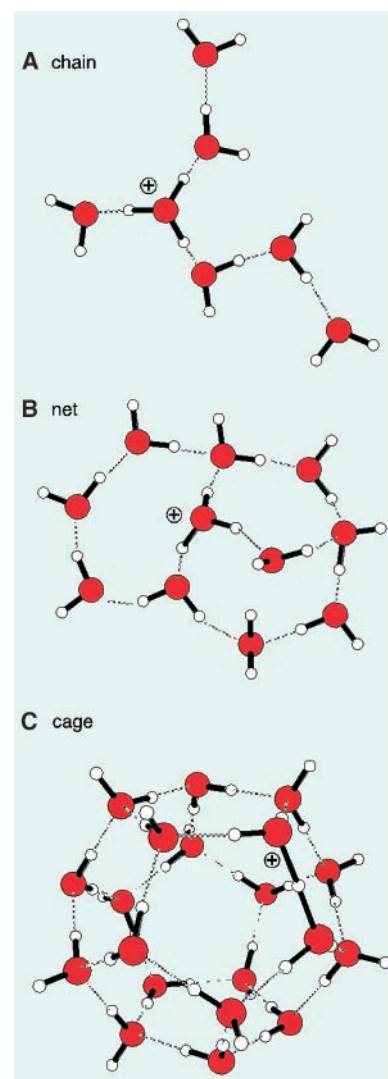

Fig. 3. A schematic representation of the development of hydrogen bond network structure with increasing cluster size. (A) Chain structure in $n \lesssim 10$. (B) Two-dimensional net structure (~10 < n < 21). (C) Three-dimensional cage structure in $n \geq 21$.

the other AD-water molecule to form an AAD-water molecule with the acceptance of one more proton. As schematically shown in Fig. 3C, when all of the water molecules are three-coordinated (AAD and ADD), the hydrogen bond network should have a 3D cage structure in which each water molecule is located at the vertex of the polyhedral cages, because of the tetrahedral coordination nature of the water hydrogen bond. On the basis of mass spectrometry and ab initio calculations, the structure of cluster $n = 21$ has been suggested to be a regular dodecahedron cage that includes one water inside the cage ($1, 2, 9, 10$). Many nearly isoenergetic structural isomers, including the 2D net types, may contribute to the present IR spectra because of the internal energy of the clusters. However, the dominance of the AAD dangling OH band intensity over the AD dangling OH band intensity in $n \geq 21$ clearly indicates that the 2D net types are converted to 3D cage structures in this size region. Such nanometer-sized cage structures have not previously been experimentally confirmed for hydrogen-bonded cluster systems. The central H_3O^+ or $H_5O_2^+$ ion core prefers the planar coordination by nature, and it allows 3D cage formation only in such large-sized clusters.

References and Notes

1. U. Nagashima, N. Nishi, H. Tanaka, *J. Chem. Phys.* **84**, 209 (1986).
2. S. Wei, Z. Shi, A. W. Castleman Jr., *J. Chem. Phys.* **94**, 3268 (1991).
3. T. F. Magnera, D. E. David, J. Michl, *Chem. Phys. Lett.* **182**, 363 (1991).
4. N. F. Dalleska, K. Honma, P. B. Armentrout, *J. Am. Chem. Soc.* **115**, 12125 (1993).
5. L. I. Yeh, M. Okumura, J. D. Myers, J. M. Price, Y. T. Lee, *J. Chem. Phys.* **91**, 7319 (1989).
6. M. Okumura, L. I. Yeh, J. D. Myers, Y. T. Lee, *J. Phys. Chem.* **94**, 3416 (1990).
7. J.-C. Jiang *et al.*, *J. Am. Chem. Soc.* **122**, 1398 (2000).
8. S. J. Singer, S. McDonald, L. Ojamäe, *J. Chem. Phys.* **112**, 710 (2000).
9. A. Khan, *Chem. Phys. Lett.* **319**, 440 (2000).
10. M. P. Hodges, D. J. Wales, *Chem. Phys. Lett.* **324**, 279 (2000).
11. F. Huisken, M. Kaloudis, A. Kulcke, *J. Chem. Phys.* **104**, 17 (1996).
12. K. Liu *et al.*, *Nature* **381**, 501 (1996).
13. R. N. Pribble, T. S. Zwier, *Science* **265**, 75 (1994).
14. M. Miyazaki, A. Fujii, T. Ebata, N. Mikami, *Phys. Chem. Chem. Phys.* **5**, 1137 (2003).
15. Protonated water clusters were produced by a photo-assisted discharge of water vapor seeded in Ne (total pressure 3 atm). The gas mixture was expanded from a pulsed supersonic valve through a channel nozzle (*23*). The channel was equipped with a wire electrode at its sidewall, and a dc voltage of −300 V relative to the channel was applied to the electrode. The discharge in the channel was triggered by irradiation of the electrode surfaces with a laser pulse (355 nm, ~5 mJ/pulse), which was synchronized with the pulsed valve operation. The protonated water cluster cations were cooled on expansion from the channel. The size distribution of the produced cluster cations was similar to those reported so far (*1*), and the magic number at $n = 21$ was also seen.
16. We observed that 3 to 10% of the parent-cluster cations spontaneously dissociate after passing through the first quadrupole mass filter. Evaporation of one water molecule was the unique dissociation pass.
17. V. Buch, J. P. Devlin, *J. Chem. Phys.* **94**, 4091 (1991).
18. J. C. Jiang *et al.*, *Chem. Phys. Lett.* **289**, 373 (1998).
19. B. Rowland, M. Fisher, J. P. Devlin, *J. Chem. Phys.* **95**, 1378 (1991).
20. C. J. Gruenloh *et al.*, *Science* **276**, 1678 (1997).
21. U. Buck, I. Ettischer, M. Melzer, V. Buch, J. Sadlej, *Phys. Rev. Lett.* **80**, 2578 (1998).
22. J. P. Devlin, J. Sadlej, V. Buch, *J. Phys. Chem. A* **105**, 974 (2001).
23. S. Sato, T. Ebata, N. Mikami, *Spectrochim. Acta* **50A**, 1413 (1994).
24. We are grateful to H. Ishikawa and T. Maeyama for useful discussions and to H. Kawamata for his contribution to the IR laser system construction.

Infrared Signature of Structures Associated with the $H^+(H_2O)_n$ ($n = 6$ to 27) Clusters

J.-W. Shin,[1] N. I. Hammer,[1] E. G. Diken,[1] M. A. Johnson,[1]* R. S. Walters,[2] T. D. Jaeger,[2] M. A. Duncan,[2]* R. A. Christie,[3] K. D. Jordan[3]*

We report the OH stretching vibrational spectra of size-selected $H^+(H_2O)_n$ clusters through the region of the pronounced "magic number" at $n = 21$ in the cluster distribution. Sharp features are observed in the spectra and assigned to excitation of the dangling OH groups throughout the size range $6 \leq n \leq 27$. A multiplet of such bands appears at small cluster sizes. This pattern simplifies to a doublet at $n = 11$, with the doublet persisting up to $n = 20$, but then collapsing to a single line in the $n = 21$ and $n = 22$ clusters and reemerging at $n = 23$. This spectral simplification provides direct evidence that, for the magic number cluster, all the dangling OH groups arise from water molecules in similar binding sites.

The nature of the proton in water is one of the most fundamental aspects of aqueous chemistry, and one important aspect of the aqueous proton is its anomalously high mobility (*1, 2*). This phenomenon immediately introduces the crucial role of H_3O^+ and $H_5O_2^+$, the so-called Eigen (*3*) and Zundel (*4*) forms of the cation, respectively. Fluctuations between these species (*1, 2*) are thought to mediate the Grotthuss mechanism (*5*) for proton transport, and accurate simulations of this process require quantum treatment of the hydrogen motion in the complex network environment of bulk water.

A powerful way to test the validity of various theoretical methods is through the use of cluster ions (*6*), $H^+(H_2O)_n$, which can be prepared and isolated in the laboratory. Here, we report size-selected vibrational spectra of the $H^+(H_2O)_n$ clusters in the intermediate size regime, $6 \leq n \leq 27$, chosen to explore the putative role (*7–12*) of dodecahedral clathrate structures in the region around $n = 21$. The resulting spectra are analyzed with the aid of calculated structures and vibrational frequencies of selected isomers for the $n = 20$ and $n = 21$ clusters.

Protonated water clusters have been stud-

[1]Sterling Chemistry Laboratory, Yale University, Post Office Box 208107, New Haven, CT 06520, USA. [2]Department of Chemistry, University of Georgia, Athens, GA 30602, USA. [3]Department of Chemistry, University of Pittsburgh, Pittsburgh, PA 15260, USA.

*To whom correspondence should be addressed. E-mail: mark.johnson@yale.edu (M.A.J.); maduncan@uga.edu (M.A.D.); jordan@imap.pitt.edu (K.D.J.)

ied for decades (*3, 4, 7–18*), and in the small size regime ($n \leq 8$) vibrational spectra have been reported and interpreted with ab initio theory (*17*). H_3O^+ itself is C_{3v} pyramidal (*13*), but adding a second water molecule leads to a symmetrical sharing of the proton in the $H_2O\cdots H^+\cdots OH_2$ Zundel arrangement (*4, 18*). Larger protonated water clusters possess multiple low-energy isomers with both Eigen and Zundel forms of the cation, and the complexity of the observed spectra indicate that several isomers are present under experimental conditions.

One of the most curious aspects of the $H^+(H_2O)_n$ clusters is Searcy and Fenn's (*7*) report in 1974 of the discontinuity in the cluster ion intensity distribution or "magic number" at $n = 21$ (Fig. 1). There has been much speculation about the structure of the magic number cluster, especially because water clathrates are known to trap methane and other gases in water cages composed of water dodecahedrons (*19*). Indeed, Searcy and Fenn (*7*) suggested that $H^+(H_2O)_{21}$ is also derived from the pentagonal dodecahedron motif, with one water molecule in the cage and the H_3O^+ ion on the surface.

In 1991, Castleman and co-workers reported a "titration" of dangling H atoms by attaching trimethylamine (TMA) molecules to the $H^+(H_2O)_{21}$ cluster (*9*). They found a drop-off in the propensity to attach the 11th TMA molecule, which suggested that 10 H atoms are free (i.e., not engaged in H-bonding) in the $H^+(H_2O)_{21}$ cluster. Because this is the same number as in the